An overview of multiple DoF magnetic actuated micro-robots.

Soukeyna Bouchebout, Aude Bolopion, Jean-Ochin Abrahamians, Stéphane Régnier

Noname manuscript No.
(will be inserted by the editor)

An overview of multiple DoF magnetic actuated micro-robots

Soukeyna Bouchebout · Aude Bolopion · Jean-Ochin Abrahamians · Stéphane Régnier

Received: date / Accepted: date

Abstract This paper reviews the state of the art of untethered, wirelessly actuated and controlled micro-robots. Research for such tools is being increasingly pursued to provide solutions for medical, biological and industrial applications. Indeed, due to their small size they offer both high velocity, and accessibility to tiny and clustered environments. These systems could be used for *in vitro* tasks on lab-on-chips in order to push and/or sort biological cells, or for *in vivo* tasks like minimally invasive surgery and could also be used in the micro-assembly of micro-components. However, there are many constraints to actuating, manufacturing and controlling micro-robots, such as the impracticability of on-board sensors and actuators, common hysteresis phenomena and nonlinear behavior in the environment, and the high susceptibility to slight variations in the atmosphere like tiny dust or humidity. In this work, the major challenges that must be addressed are reviewed and some of the best performing multiple DoF micro-robots sized from tens to hundreds μm are presented. The different magnetic micro-robot platforms are presented and compared. The actuation method as well as the control strategies are analyzed. The reviewed magnetic micro-robots highlight the ability of wireless actuation and show that high velocities can be reached. However, major issues on actuation and control must be overcome in order to perform complex micro-manipulation tasks.

Keywords micro-robot · magnetic actuation · control

1 Introduction

The promising field of micro and nano technologies based on wirelessly powered and maneuvered submillimeter devices has recently been developed. As these micro-robots have a small size and are untethered, they can fit in fluidic systems and manipulate micro-objects, likewise they can experience very high velocities and carry out many actions in a short time. Several areas will benefit from these advanced technologies.

As for potential applications, advanced manufacturing relies on the micro-assembly of small mechanical components, using micro-agents manipulating micro-objects in order to build assembled systems. For example, Micro-Opto-Electro-Mechanical Systems (MOEMS) sense or manipulate optical signals on a very small size scale using integrated mechanical, optical, and electrical systems, therefore their fabrication requires a precise micro-assembly system. Another example is the fabrication, packaging and interconnection of different micro-components in the MEMS (Micro-Electro-Mechanical-Systems) where micro-assembly is vital. Modular robotics can also benefit from micro-robotics. Reducing the size of individual robotic modules increases the spatial resolution of reconfigurable robots, hence it adds to their versatility and range of tasks. Industrial biotechnology and medicine are also suitable fields for micro-robot use. Indeed, micro-robots operate at the same scale as organic cells, allowing efficient *in vitro* interaction in order to move and/or sort cells. Hence they can fit in lab-on-chips and perform adaptable tasks on corpuscles such as blood cells sized from 6 to 10 μm. Minimally Invasive Surgery (MIS) greatly reduces patient trauma and time recovery through the use of smaller tools, in the future micron-sized robots could

Soukeyna Bouchebout · Jean-Ochin Abrahamians · Stéphane Régnier
Institut des Système Intelligents et de Robotique (ISIR), Université Pierre et Marie Curie/CNRS UMR- 7222, BC 173, 4 Place Jussieu, 75005 Paris, France E-mail: bouchebout@isir.upmc.fr

Aude Bolopion
FEMTO-ST Institute, UFC, ENSMM, UTBM, CNRS UMR-6174, 24 rue Alain Savary, 25000 Besançon France

be inserted in the human body to reach locations that conventional surgery can't access [1], and used in targeted drug delivery to sickly cells or tumors.

The reduced size makes it impractical to power micro-devices through built-in energy sources, as they are currently hard to achieve at this scale. However, offboard actuation processes can be used that cannot be applied on macro scale systems. Significant progress has been realized in this regard using various methods. The electrostatic effect [2] powers scratch drive actuators, although these devices need a patterned surface to operate on. The dielectrophoresis forces generated by an electric field can also be used to position a micro dielectric particle [3], however this method provides short courses for the micro-devices. Magnetostrictive actuation [4] relies on robot deflection to create motion, although predicting the magnetostrictive behavior is critical to these systems. Piezo-electric actuation [5] relies on the robot distorting to create motion but requires a high voltage. Thermal actuation [6], while unsuitable for biological purposes, would be adapted to actuate submillimiters devices - since thermal capacity depends on volume, heating and cooling times are greatly reduced for micro-devices [7]. The main difficulty for thermal actuators is to apply and measure two different temperatures locally in a controlled manner [8]. Biological properties can also be used to actuate micro-robots, like bacteria's properties [9] [10] which present great potential for future research in drug delivery. The main issue with these systems is to maintain low cytotoxicity induced by the bacteria while the detection and required payloads are guaranteed. Other actuation methods can be used such as laser beams [11] [12], but this method offers a low range of forces ∼pN. Electromagnetism can be used as a power source in several ways. Swimming micro-robots [13] [14] [15] employ magnetic actuation as a propulsion method in a fluidic environment: the micro-robot is wirelessly pulled. Though, the swimming micro-robots can be fitted with helical propellers [16] [17] [18] . These micro-robots are well suited for *in vivo* medical applications. The Magnetically driven MicroTool (MMT) which showed good performances in interacting with biological cells [19] also uses magnetic actuation, usually with permanent magnets. The MMT is mainly aimed to fit in fluidic systems to perform a specific task on cells. Moreover, various mobile micro-robots use electromagnets as power sources [20], [21] [22]. As the most often magnetic micro-robots used are made of a soft magnetic material, both a high magnetic gradient and magnetic field magnitude are suitable. However, the systems providing high homogeneous magnetic field with a weaker magnetic gradient, like the Magnetic Resonance Imaging (MRI) benefit from a large workspace but are limited in DoF. Whereas, the electromagnetic systems allowing high DoF within a smaller workspace, lake of magnetic field homogeneity and use high gradient field or larger volume of micro-robots. Such compromises are critical in the electromagnetic systems and can be addressed according to the micro-robot application. These systems can perform tasks both in dry and wet surfaces. The magnetically actuated micro-robots are force-controlled with position feedback, in contrast with macro scale robotic tools which are position-controlled with force sensing or visual feedback. Thus limitations on generated forces can be imposed to allow, besides performing industrial tasks, safe interactions with living biological micro-objects. Regarding the advantages of magnetic actuation, this review approaches magnetically actuated micro-robots.

The aim of this review is to highlight the main challenges facing magnetically actuated micro-robots, and solutions that have been proposed through some examples of the most successful magnetic actuated micro-robots. The systems discussed in this work are restricted to untethered micro-robots sized between tens to hundreds μm that can generate important forces compared to their reduced size. The addressed systems can be considered as multipurpose, accessible, i.e. simple fabrication processes, and having more than one degree of freedom (DoF). These micro-robots are actuated by electromagnets as they offer a convenient control system by current signals. The four systems considered in this paper are: the Mag-μBot from Carnegie Mellon University, the OctoMag of the ETH Zurich, a paramagnetic particles control system from the University of Twente, and the MagPieR of the ISIR and FEMTO-st laboratories. There are many challenges in achieving such systems. The design of magnetic micro-robot systems is divided between designing the actuators, and the microfabrication of the micro-robots. Currently, dimensioning the electromagnets and optimizating their configuration are among the concerns in designing the systems. Besides, the manufacturing of micro-robots is today possible with the emergence of new micro fabrication techniques, however controlled surface conditions are difficult to achieve. Moreover, the challenge in fulfilling micro-robotic applications is to have the ability to position, and for anisotropic shapes orientate, micro-robots with micron accuracy, in order to interact with micro-objects. Hence, a robust and efficient control system is required, more so because of the nonlinearities that occur at the micro scale: predominant adhesion forces, significant hysteresis phenomena, and the high sensibility of micro systems to environment variables, such as humidity, residues, dust etc. The control system must be robust to these environment noises, and as the micro world allows for very high velocities, a fast control response is also required. Therefore, a good compromise between command robustness and speed is critical. In addition to these environment-related drawbacks, on-board sensors or controllers are hard to achieve on micro-robots due to the small scale. Thus, a fast and efficient external sensing and motion tracking method is needed to locate the micro-robot. Several detection methods can be used,

like cameras [21], X-rays, laser scanning, MRI [23] [24] [25], and fluoroscopy. The choice of the imaging systems is important and depends on the environment of the micro-device, range of detection field, cost, tracking speed and flexibility. Perception feedback can be exploited by a user in a teleoperation mode while the control system enhances manipulating precision at a micro scale, as is ideally the case for MIS. Camera frames can also be used in a fully automated manner, which is required for autonomous industrial micro-assembly or operations on cells due to the high number of repetitive tasks.

This work is organized as follows. Section 2 details the major challenges that need to be addressed. Sections 3, 4, 5, 6 illustrate how four micro-robot systems, the Mag-μBot from Carnegie Mellon University, the OctoMag of the ETH Zurich, a paramagnetic particles control system from the University of Twente, and the MagPieR of the ISIR and FEMTO-st laboratories, approach micro-robotic challenges, with focus on the micro-robot platforms, motion mechanisms and force/position controls. This review is concluded in section 7 with a comparison between the discussed systems.

2 Challenges of magnetically actuated micro-robots

Usually, the studied magnetic micro-robots systems consist in electromagnets surrounding the micro-robot workspace, as depicted in fig. 1. The micro-robot evolves in a workspace we will call the arena, which can include a fluid (liquid or gas). The scene is observed using a camera fitted with a microscope objective. In this section the main issues in designing, actuating and controlling such systems are discussed.

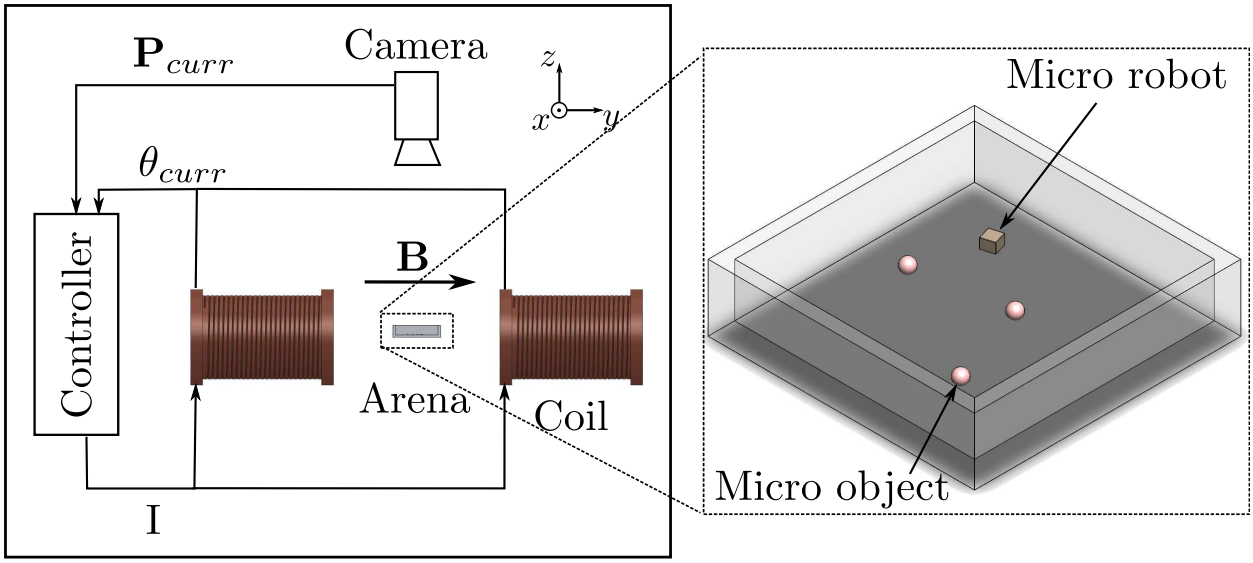

Fig. 1 An example of a magnetic actuated micro-robot

2.1 Challenges of magnetic micro-robot actuation

An object with a non-zero internal magnetization experiences magnetic forces and torques when exposed to a magnetic field **B**, and thus exhibits motion [26]. **B** [T] is characterized by its directions represented as field lines, and by its value called flux density. It is a function of the magnetic **H** [T] field called field strength. It is proportional to the magnetization field **M** [A m] of its source, which is the density vector field of local magnetic moments inside its volume V. The magnetic moment $\mathfrak{m}$ [A m^2] is a vector quantity resulting from the motion of charges within a magnetized object, and describes its ability to magnetically interact with other magnetized objects or magnetic fields.

Several types of magnetized materials can be used [27]. In ferromagnetic and ferrimagnetic materials, magnetic domains locally regroup large numbers of atomic magnetic moments, which describes an element's ability to

magnetically interact with magnetized objects or magnetic fields, pointing towards the same directions. These magnetic domains result in an overall magnetic moment in permanent magnets, or compensate each other in other materials. An external magnetic field can realign these magnetic domains according to its directions which may result in forces and torques on the object : these materials are attracted towards stronger values of the magnetic field. The stronger the exciting field is, the more magnetic domains realign, until it reaches magnetic saturation as all the domains point towards the same direction. Thus, a ferromagnetic object which produces no magnetic field on its own can also be used to enhance an external magnetic field. Residual magnetization may remain when the exciting field is switched off, and may be permanent. Ferromagnetic and ferrimagnetic materials are classified as soft magnetic if the remaining magnetization is small and dissipates very fast, which is suitable for use in micro-robotics, or hard magnetic when residual magnetization is significant, which can produce permanent magnets. The advantage of using ferromagnetic micro-robots is to generate significant forces that can be used in the assembly or handling of micro-components.

Other materials are susceptible to magnetic fields, like paramagnetic and diamagnetic materials. These materials do not possess magnetic domains and are not subject to magnetic remanence, but magnetic moments linked to their unpaired electrons for paramagnetic materials, or paired electron orbital motions for diamagnetic materials, can likewise realign in the presence of a magnetic field. Paramagnetic materials realign their magnetic moments in the direction of $\mathbf{B}$, while diamagnetic materials realign their magnetic moments in the opposite direction of $\mathbf{B}$. Hence, a diamagnetic micro-device can benefit from a point of equilibrium; which is suitable for the control. Diamagnetism can be observed in all materials, but is very weak except in superconductors : when paramagnetic properties exist they prevail over diamagnetic repulsion. Paramagnetic materials themselves present a much weaker attraction towards stronger values of the magnetic field than ferromagnetic materials, and therefore require a stronger magnetic source to achieve similar results.

In practice, to express the forces exerted by a magnetic field on a ferromagnetic object, constant experimental values can be used as a uniform magnetization $\mathbf{M}$ for unsaturated materials. While, on a paramagnetic body, the local magnetic moment is proportional to the applied magnetic field, where α is the proportionality constant measured by a magnetometer. The magnetic force $\mathbf{F}_m$ relies on the non-uniformity of the magnetic field $\mathbf{B}$ and is proportional to the magnetic field gradient. The magnetic torque $\mathbf{T}_m$ is proportional to the magnetic field and acts to bring the internal magnetization of an object into alignment with the field. The magnetic forces and torques are expressed in Tab. 1for both ferromagnetic and paramagnetic material.

Material	$\mathfrak{m}$	$\mathbf{F}_m$	$\mathbf{T}_m$
Ferromagentic	$\mathfrak{m} = \mathbf{M}\mathrm{V}$	$\mathbf{F}_m = \mathrm{V}(\mathbf{M}\cdot\nabla)\mathbf{B}$ (1)	$\mathbf{T}_m = \mathrm{V}\mathbf{M}\times\mathbf{B}$ (2)
Paramagnetic	$\mathfrak{m} = \alpha\mathrm{V}\mathbf{B}$	$\mathbf{F}_m = \alpha\mathrm{V}\cdot\nabla(\mathbf{B}^2)$ (3)	$\mathbf{T}_m = 0$

Table 1 Summary of the magnetic forces and torques on ferromagnetic and paramagnetic materials

Regarding the effect of $\mathbf{B}$ on magnetic materials, the magnetic field can be employed to actuate micro-robots made of a magnetic material. $\mathbf{B}$ fields can be used to actuate micro-robots in several ways. Stick-slip motion induced by magnetic torques can produce translation [28]. In addition to the stick-slip method, magnetic forces can produce a rolling motion on spherical magnetic micro-bodies [29]. Using magnetic forces as a direct propulsion method requires a stronger magnetic field to move the micro-device [21], but generates higher magnetic forces when interacting with micro-objects. Besides, magnetic forces can be used to create vibrations in a micro-robot [30] [31] [32], leading to motion at its resonance mode. In the case of the magnetically actuated systems purposed for *in vivo* or *in vitro* biomedical applications, the biocompatibility of magnetic materials is important for such magnetic systems. Coating the magnetic material with polymer layers [33] can be used, to prevent the magnetic materials from corrosion and leaching. Moreover, some biocompatible magnetic materials exist [34] but there biocompatibility is limited in time.

2.2 Challenges in designing magnetic actuation platforms and micro-robots

The addressed magnetic actuation systems are based on electromagnets which generate a magnetic field $\mathbf{B}$ by applying a current I. The linearity and the strength of $\mathbf{B}$ depends on the input I and the coil parameters, like the number of loops, size, geometry and core of the electromagnet. Designing magnetic micro-robots involves the optimization of the electromagnets' parameters, thus maximizing the workspace and DoF of the micro-robots, the

generated forces while manipulating micro-objects, as well as minimizing the latency and non-linearities of the coils for a fast and robust control of the micro-robots.

As **B** can be controlled by I, its intensity can be increased or turned off. Besides, the current signal can be modulated through software and can exhibit different forms: sinusoidal, sawtooth, square, triangle etc.. Thus, different magnetic fields can be produced to obtain trajectory control. The maximum admissible current intensity in the electromagnet depends on how much heat the conductive material can withstand and how fast it can be dissipated by the coil. However, cooling systems [21], or square waveform current instead of continuous current [35] can be used.

Besides, the strength and linearity of the magnetic field depend on the core of the coil. The field generated by a coil without a core (air-core) Fig. 2(a) is directly proportional to the applied current intensity. The generated magnetic field is strongest inside the coil, and falls off rapidly outside of its volume. It is then important to keep the micro-robot as close as possible to the coil, which restrains its workspace. However, it is possible to generate a stronger magnetic field outside of the electromagnet by adding a soft magnetic core at its center Fig. 2(b). If the core reaches magnetic saturation the magnetic field is no longer proportional to the current intensity input.

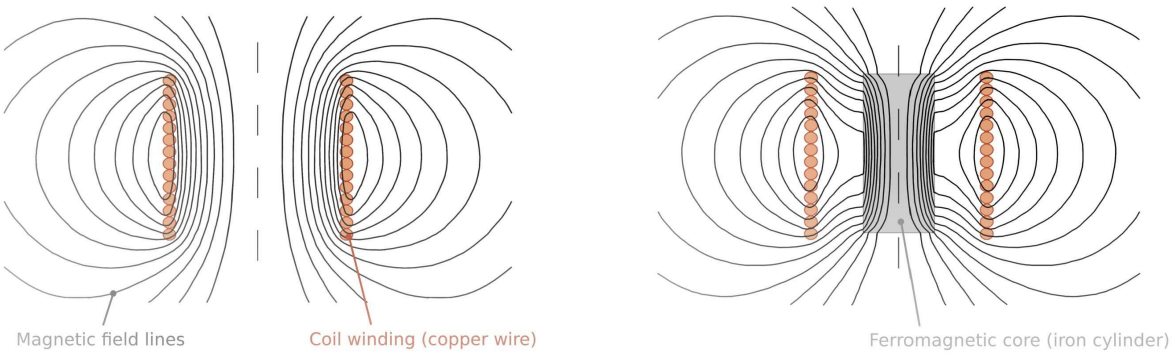

(a) Air core electromagnet magnetic field lines.

(b) Iron core electromagnet magnetic field lines.

Fig. 2 Field lines comparison between an air core and iron core electromagnet. Data obtained by FEMM software [1].

In order to improve the micro-robot DoF, several fixed electromagnets can be controlled to produce different fields one at a time, or more complex fields when combined. The resulting field can then be considered as the linear superposition of the effects of each individual electromagnet for air-core coils, even though a very weak mutual induction exists between the coils. This approximation can also be applied to ferromagnetic core coils, as long as the sources are far enough from each other for the field generated by an electromagnet not to affect another's core [21]. The challenge in choosing the coils configuration and micro-robot DoF is to reduce the distance between the electromagnets and the micro-robot to increase the available magnetic field strength, while keeping a certain distance to avoid overwhelming nonlinearities. Moreover, as one coil induces displacement of the micro-robot in one direction, the number of the used coils and their configuration influences the DoF of the micro-robot. Thus, to obtain controlled 2D motion at least 4 coils are needed, and for 3D fully controlled motion a minimum of 6 coils is required. Some typical configurations can be used in the design. For example, in a method of actuation relying on propulsion, Helmholtz coils[2] generate a uniform magnetic field intensity near the center of the coil to align the micro-robot located near the center of the coil along the coil's axis, and Maxwell coils[3] are used to generate a uniform gradient magnetic flux and propel the micro-robot in the desired direction [36]. However, due to the electromagnets' size, the admissible configurations are restrained. This can be tackled by using a dynamic configuration of the coils i.e. moving the electromagnets [37].

Once the macro scale actuation system is designed, the micro-robot fabrication can be addressed. Magnetic micro-robots are usually made of ferromagnetic materials and have more or less simple geometric shapes depend-

[1] http://www.femm.info/

[2] Helmholtz coil pair: two identical circular magnetic coils placed symmetrically one on each side along a common axis, and separated by a distance equal to the radius of the coil. Each coil carries an equal electrical current flowing in the same direction.

[3] Maxwell coil pair: two identical circular magnetic coils placed symmetrically one on each side along a common axis, and separated by 1.73 times their radius. Each coil carries an equal electrical current flowing in the opposite direction.

ing on their intended purpose; for example they can have a crescent shape to clasp micro-devices. Micro-robots are sized from tens to hundreds μm. Since adhesion forces at this scale are very high and depend on surface roughness, the manufacturing method should offer accurately controlled micro-robots surfaces. To machine such micro-devices, macro scale processes can be used such as laser fabrication. Micro-fabrication process like lithography can also be used in machining micro-devices. Laser fabrication consists in cutting a large stock of a material using a small laser spot, whereas lithography-based fabrication combines operations of selective deposition and growth of materials, like sputtering, chemical vapor deposition, electroforming, spin-coating, etc., and selective removal, such as deep-reactive ion etching (DRIE). Lithography allows machining micro-objects with layers of different materials, and guarantees a smoother surface than laser fabrication, however the latter preserves magnetization and density values of the material which is not the case with a lithography-based process. The challenge for future magnetic micro-robots is to include internal DoF, like active clamps which can be actuated independently to perform complex micro-manipulation tasks.

2.3 Challenges in controlling magnetic micro-robots

The first step in controlling micro-robots is to perform open loop control. The user applies a given I to bring the micro-robot to a desired position $\mathbf{P}_{des} = [x_{des}\ y_{des}]^{\mathrm{T}}$ in 2D [4]. An I applied through a coil generates a magnetic field $\mathbf{B}$, the magnetic field applies a magnetic torque on the micro-robot following Eq. (2) and a magnetic force according to Eq. (1).The orientation of the device θ_{curr} is commonly assumed to be equivalent to the magnetic field orientation [21], but the translation of the micro-device needs to be identified. The control of the magnetic micro-robot can be based on I or $\mathbf{B}$. In both cases, knowledge of the relation between the micro-robot velocity and the electric current input I or the magnetic field $\mathbf{B}$ is essential. Controlling magnetic micro-robots with $\mathbf{B}$ relies on the evaluation of $\mathbf{B}$ using hall sensors. In this case these sensors can be integrated all over the arena surface which is costly. However, they can be placed next to the coils and by interpolation, estimate $\mathbf{B}$. Besides, the latency of the hall sensors should be minimal to perform fast control. When controlling the micro-robot through I, the identification of the generated $\mathbf{B}$ by a current I flowing in the coil is important and must include the latency and the non linearity of the coil. This identification can be performed by an analytic model, which does not take all the coil properties into account, or by a finite elements model (FEM), which is calculated off-line and cannot be used in a real-time fashion. However, the combination of the two methods is possible, i.e. simulating the response off-line and then integrating it in an analytic model for real-time computation.

In addition to the identification of the coil parameters, the computation of the direct/inverse model system, i.e the relation between the micro-robot velocity and $\mathbf{B}$/I, or vice versa, is one of the main issues in controlling magnetic micro-robots. Actually, magnetic forces can induce the same accelerations regardless of the object's size, therefore a micro-robot can experience high accelerations relative to its reduced size However, depending on the environment, the micro-robot's behavior is disturbed by high adhesion forces in the air [38], which depends closely on the surface of the arena and fabrication of the micro-robot. Adhesion forces can be reduced at this scale by using vibrations generated from a piezoelectric layer [35], or levitation using the electrostatic effect. In a liquid environment, the micro-robot experiences fluid drag forces [38], which increase with its velocity; as the micro-robot operates, the liquid state changes and leads to system disturbances. Besides liquid drag forces, the micro-robot can experience adhesion forces if it sticks to the surface. To reduce or avoid surface adhesion forces in liquid, the surface of the micro-robot can be adapted to make it float [37]; or it can be maintained in the fluid above the surface by capillary forces [22]. The challenge in identificating the behavior of magnetic micro-robot systems lies in the significant influence of non-linearities, although systems parameters can be evaluated theoretically and corrected by several repeatable experiences. Other methods can be used such as neural networks [39] or learning machines [40], which showed good performance in identifying macro scale nonlinear systems.

To provide autonomy and time gain to the user, a closed loop system is required. In this case, the controller automatically computes the I needed to reach the desired position $\mathbf{P}_{des}$. Due to the reduced size of the robot, mounted sensors are impractical. The micro-robot position $\mathbf{P}_{curr} = [x_{curr}\ y_{curr}]^{\mathrm{T}}$ can be detected using various sensors. Although, cameras are widely used due to the low cost and fast computational time. The camera should be fast enough (several hundreds of Hertz at least) to ensure a stable control law. The image processing can benefit from the contrast between the micro-robot and its background environment, for example by applying threshold and/or morphological operations on arena captions. Predictive control is suitable to speed up the control loop. Besides, other detection methods can be used such as event-based sensors, which are faster but have a more

[4] Respectively $\mathbf{P}_{des} = [x_{des}\ y_{des}\ z_{des}]^{\mathrm{T}}$ in 3D

complex processing and need to be calibrated with a classic camera. Event-based sensors mimic biological visual systems and react to changes of contrast that are converted in a stream of asynchronous time-stamped events [41]. The controller uses the value returned by the detection method, and according to the desired position sets the input to the electromagnets. It thus minimizes the error ε_* [5], which is the difference between the current and desired position values. The control of the micro-robot system is achieved by specific software according to the tasks to be executed. Thus, the control of magnetic micro-robots, besides avoiding obstacles and performing trajectories, has to be adapted to the micro-robots' tasks. Clearly, micro-objects manipulation differs depending on the environment. In the air, the micro-robot needs to generate important forces to push/pull micro-devices and contract the adhesion forces, whereas in liquid the control of the micro-robot needs to adapt to the fluid movement carrying the micro-objects. Besides the control of one micro-object, controlling multiple micro-robots in cooperation may allow to perform more complex tasks, like handling a bigger object, and cooperatively handle an object.

In the following sections, four magnetic micro-robots are presented, and the approaches proposed to handle the above mentioned challenges are highlighted.

3 Mag-μBot (Magnetic micro roBot)

3.1 Micro-robot design

The Mag-μBot was introduced in [20] [42]. The system contains six identical electromagnetic coils in an orthogonal configuration. The coils surround the arena, wherein resides the magnetic micro-robot (Mag-μBot) Fig. 3(a). The maximum generated magnetic field and gradient field are respectively around 15 mT and 0.65 T.m^{-1}, these values being measured at the center of the arena. A camera is located inside the top electromagnet. It is a classic CCD camera coupled with a variable magnification microscope lens providing a field of view of 26 mm $\times$ 20 mm.

A Mag-μBot is a composite of Neodymium-Iron-Boron. Two fabrication processes can be used in machining Mag-μBots. First, a laser micro-machining system has been used in the fabrication of the Mag-μBot [20]. The second process relies on batch manufacturing using molding techniques. The micro size moulds are produced by a lithography based process. The process allows the production of large numbers of Mag-μBots. To handle micro-components, the micro-robot's shape can be adapted. Thus, the Mag-μBots is fabricated in several shapes (parallelepiped, cylinder etc.). Fig. 3(b) depicts the Mag-μBots with claws to manipulate micro-objects.

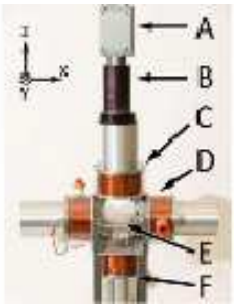

(a) Picture of the Mag-μBot system, A: Camera, B: Microscope,C: Top coil, D: Upright coil, E: The arena, F: Bottom coil [42].

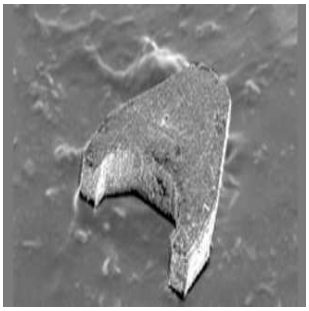

(b) The claw model of Mag-μBot: 300 μm x 300 μm x 100 μm [43].

Fig. 3 The Mag-μBot system design

3.2 Micro-robot actuation

The Mag-μBot's movement is produced by applying a time varying magnetic field. Thus the Mag-μBot exhibits a non-uniform rocking behavior, which results in a stick-slip motion across the arena surface as shown in Fig.

[5] ε_x, ε_y, ε_z, ε_θ, are respectively the error along x, y, z direction and the orientation.

4. However, this composite motion limits the velocity of the Mag-μBot. The orientation of the micro-robot is produced by one of the in plane coils, while the Mag-μBot is held down by the magnetic field generated by the bottom coil. The translation of the micro-robot is achieved by out-of-plane pulses. The top coil applies an alternating magnetic field leading the micro-robot to rock downward when the field decreases, and upward when it increases, and due to surface friction the micro-robot experiences stick and slip phases which result in translating movement. As the motion of the Mag-μBot is composed of rotations, the torques are responsible for the micro-robot going forward or rotating. The magnetic torques are given by Eq. (2). As the movement of the Mag-μBot is based only upon magnetic torques, the system requires a much smaller magnetic field strength than magnetic gradient-based systems (i.e magnetic force-based systems). The velocity of the Mag-μBot can reach 25 mm.s^{-1}, as performed at the NIST IEEE Mobile Microrobotics 2010 Challenge [44].

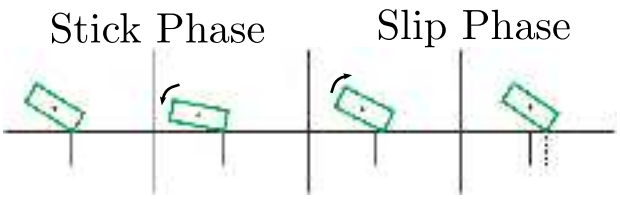

Fig. 4 Mag-μBot performing a translation. The solid line is the initial micro-robot position, the dotted line is the position of the micro robot after movement. In the stick phase the micro-robot is stationary because of surface friction, as soon as the contact between the micro-robot and the surface slips, the Mag-μBot translates. [28] .

3.3 Motion control

In order to servo the system, a correlation is set up between the current signal input and the micro-robot's behavior. Simulations and experiments were done to determine the velocity of the micro-robot as a function of the signal frequency and surface roughness. Different waveform current signals (shape, frequency and amplitude varying) were applied to the system and the resulting velocities were measured from the camera frames. Thus, multiple surfaces were tested: glass, rough silicone, smooth silicone. Besides, air, vacuum and nitrogen atmospheres were tested. The Mag-μBot was also used in water, where precautions were taken to avoid the solid/liquid interface from getting the micro-robot stuck on the surface. The Mag-μBot showed lower velocities in water than in air, since the drag forces are more important in water. As the velocity of the micro-robot depends on the frequency of the current signal, values are obtained from experimental frequencies relating to the surface it operates on. Fig. 5 shows some results of these experiments and simulations. The effect of the magnetic torques is predominant compared to other forces, thus the orientation of the Mag-μBot is assumed to be equivalent to the orientation of the magnetic field in the -x,y- plane.

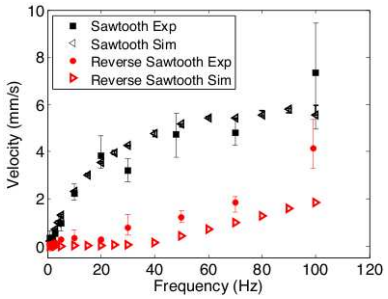

(a) Sawtooth and reverse sawtooth waveforms signal input [20].

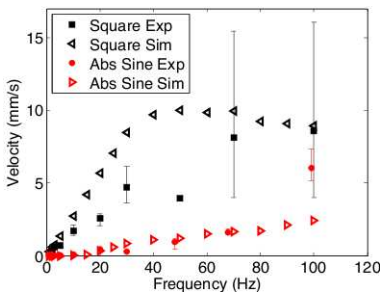

(b) Square and sine waveforms signal input [20].

Fig. 5 The Mag-μBot velocities as a function of the current signal frequency, both experimental and simulated results. The Mag-μBot is traveling on a rough silicon surface in air.

The control is performed using visual feedback. The image processing returns the current position of the micro-robot to the controller. Given the goal position, the controller sets the adequate current signal frequency and amplitude. The image processing is a particle filtering algorithm coupled with state prediction [45]. The controller is a proportional-integrator-derivative (PID), with additional imposed nonlinear logic. The nonlinear logic regulates the orientation of the magnetic field and the velocity of the robot. When too high angular accelerations are applied, the Mag-μBot can flip on its edge and its behavior becomes unknown. The aim of this block is to improve the stability of the micro-robot motion by limiting these accelerations. Fig. 6 shows the block diagram of the Mag-μBot control.

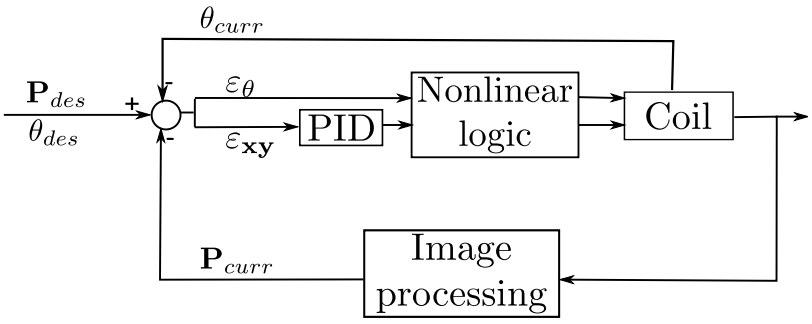

Fig. 6 Block diagram depicting the method of control for positioning a Mag-μBot to a desired goal location.

3.4 Experimental results and discussion

The reliable control of the micro-robot allows a higher level of Mag-μBot autonomy. The system is provided with a motion planner. This module computes a free collision path from an initial position to a goal position, in a clustered environment. In this case, the user defines in advance the obstacles in the environment of the robot. The planner sends to the controller the positions to follow to reach the goal and the controller generates the needed current signal to the coils. The path is computed using the Wavefront algorithm [46]. The control of the Mag-μBot generates sufficient forces and is accurate enough to perform interaction with micro-objects, such as pushing a 50 μm diameter sphere underwater. Moreover, as the Mag-μBot operates in liquid, the manipulation of micro-objects is performed using two strategies. Non-contact handling is performed using the flow-field generated by the Mag-μBot [47]. A micro-object can be also moved by direct contact, in this case the displacement of the micro-objects before contact due the flow field is significant and needs to be taken into account.

The Mag-μBot system also offers the ability to control multiple micro-robots, either by adapting the surface with electrodes and using the electrostatic effect to clamp all micro-robots except the one to move [48] [49], or by using micro-robots of different sizes, in which case each micro-robot has a specific actuation signal frequency [42]. To control the micro-robot, it must keep contact with the surface. Indeed, if the contact is broken, the robot flies during much of its travel due to the magnetic gradient. The micro-robot will then experience high velocities which are impractical for use from a controllability point of view. This behavior occurs when using the top coil, which orients the micro-robot upwards and towards the in plane coils, making the micro-robot lose contact with the surface. Hence, with this method the Mag-μBot system is restricted to 2D motion.

4 OctoMag

4.1 Micro-robot design

The OctoMag [21] micro-robot, an elliptical shaped micro-device made of Nickel-Cobalt, is surrounded by 8 soft-magnetic-core electromagnets Fig. 7. These coils can withstand a current intensity of 15 A provided by the amplifiers. The temperature in typical operating conditions is around 60^o without a cooling system, and can rise excessively if maximum magnetic forces are applied. Thus, the coils require a cooling system. The disposition of the coils were defined in order to optimize the force capability generation throughout the arena. To observe

the micro-robot, two cameras are disposed with additional optic zoom, one on the top of the arena and the other at the side of the scene. The micro-robot operates in a wet environment. The OctoMag micro-robot is a three-dimensional structure made of two micro-assembled individual parts. Micro-robot parts have been machined with electroplated nickel using a lithography process then laser cut steel [50].

Fig. 7 The OctoMag electromagnetic system. 8 soft-magnetic-core electromagnets surround the arena containing the micro-robot. A camera is fitted down the central axis to image the micro-robot [21].

4.2 Micro-robot actuation

The design of the OctoMag system allows the micro-robot to perform 6 DOF movements. However, the magnetic torque tends to align the longest axis of the micro-device with the magnetic field. Therefore, rotations along this axis are not practical, leading to the loss of one DOF. Hence, the control of the micro-robot is restricted to 5 DOF : 3 axis translation Eq. (1) and 2 rotations Eq.(2). For -n- electromagnets, each electromagnet -e- generates a magnetic field $\mathbf{B}_e$ that can be precomputed for every point $\mathbf{P}$ throughout the arena Eq. (4).

$$\mathbf{B}_e(\mathbf{P}) = \tilde{\mathbf{B}}_e(\mathbf{P}) i_e \tag{4}$$

where $\tilde{\mathbf{B}}_e$ [T.A^{-1}] is a unit-current vector and i_e[A] is a scalar current value. As the field generated by a coil is known and it is assumed that the soft magnetic core used in the electromagnets is ideal, the superposition theorem can be applied i.e the field generated by several coils is the sum of the magnetic fields generated by each coil. Thus, the magnetic field can be identified at any point of the arena as function of the current input.

$$\mathbf{B}(\mathbf{P}) = \sum_{e=1}^{n} \tilde{\mathbf{B}}_e(\mathbf{P}) i_e = B(\mathbf{P})\mathbf{I} \tag{5}$$

where $\mathbf{I}$ is a vector of the unit current i_e. As, the Octomag's micro-robot is force controlled and the force is related to $\mathbf{B}$ with Eq. (1), the derivative of the magnetic field is calculated for a given direction -x,y,z- at every point in the workspace. According to Eq. (5), the magnetic field and force is mapped through the arena for a given current signal I by the following equation:

$$\begin{bmatrix} \mathbf{B} \\ \mathbf{F}_m \end{bmatrix} = \begin{bmatrix} B(\mathbf{P}) \\ \mathbf{M}^{\mathrm{T}}\mathbf{B}_x(\mathbf{P}) \\ \mathbf{M}^{\mathrm{T}}\mathbf{B}_y(\mathbf{P}) \\ \mathbf{M}^{\mathrm{T}}\mathbf{B}_z(\mathbf{P}) \end{bmatrix} \begin{bmatrix} i_1 \\ \vdots \\ i_n \end{bmatrix} = \mathcal{A}(\mathbf{M}, \mathbf{P})\, \mathbf{I} \tag{6}$$

4.3 Motion control

The system is controlled using micro-robot position feedback from a camera. The OctoMag's micro-robot has 5 DoF, thus detection of the micro-robot in space requires two cameras. The x,y position are deduced from a top camera and the z position from a side camera. The tracking scheme of the OctoMag benefits from the use of adaptive thresholding and morphological operators, such as erosion and dilatation. The orientation of the micro-robot is controlled by an open loop assuming that if the orientation of the magnetic field is changed slowly, the

orientation of the micro-robot will be the same as the orientation of the magnetic field. Hence, the micro-robot's orientation is not measured. The magnetic field and forces are proportional to **I** Eq.(6).For a desired magnetic field and force, the current can be computed for each coil by inverting the OctoMag model:

$$\mathbf{I} = \mathcal{A}(\mathbf{M}, \mathbf{P})^{+} \begin{bmatrix} \mathbf{B}_{des} \\ \mathbf{F}_{des} \end{bmatrix} \tag{7}$$

Fig. 8 depicts the block diagram of the OctoMag.

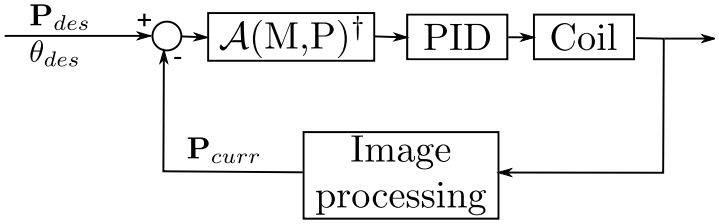

Fig. 8 Block diagram representing the method of control for positioning the OctoMag.

4.4 Experimental results and discussion

The main advantage of the OctoMag is to perform 3D motion, however only 5 DoF are fully controlled. To evaluate the precision of the OctoMag's positioning, the Octomag was controlled from a random position in the workspace to the center of the arena. Positioning of the micro-robot showed a standard deviation of 6.313, 4.757, and 8.951 μm along the x, y, and z axes, respectively, and a maximum Cartesian deviation of 29.77 μm. The positioning error was measured from 400 frames of the camera, collected at 30 Hz and the Octomag system was tested by keeping the absolute value of **B** constant (|**B**|=15 mT) to guarantee the linearization of the controller. The following figure shows a 3D ∞ shaped trajectory performed in an automated mode. Due to the positioning error, the micro-robot deviates from the desired path in some parts, however the micro-robot recovers from this drift and follows the trajectory.

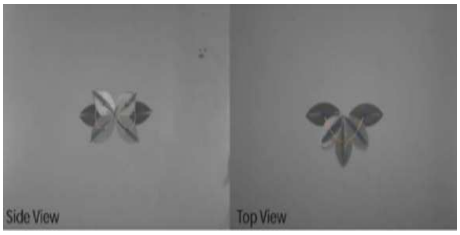

(a) The top and side view of the OctoMag's micro-robot controlled to follow an ∞-shaped trajectory. The micro-robot's orientation is kept toward the center of the sphere.

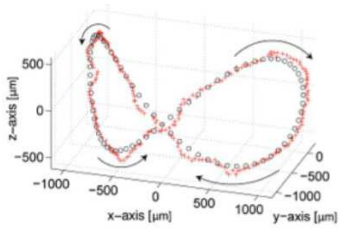

(b) This trajectory was performed in an average time of 8.3 s.The ∘ are set path points and the + are the tracked positions. The direction of displacement is shown by the arrows.

Fig. 9 OctoMag control experiments [21]

One of the potential application of the OctoMag system is to perform *in vivo* ophthalmic procedures, like the puncturing of retinal veins to inject thrombolytic drugs. Thus, the system was tested *in vitro*. It successfully performed wireless vessel puncture of blood vessels of the chorioallantoic membrane (CAM) on a growing chicken embryo, which is considered a valid test setup for applications on human retinal vessels. In this experiment, another shape of the micro-robot was used: two NdFeB cubes, of 800 μm edge, and a needle tip were glued. The overall size of the robot is more than 1600 μm in length, the device can then apply enough force to puncture vessels.

5 Magnetic control of paramagnetic particles

5.1 Micro-robot design

An image-based magnetic control of paramagnetic micro-particles system was presented in [22] and [51]. In this work, the micro-robot is a sphere of diameter ~ 100 μm made of a paramagnetic material (iron oxide). The paramagnetic particles are standards and commercially available. Four identical electromagnets are responsible for the actuation of the micro-spheres, which lie in an arena Fig. 10(a) containing a liquid (water), and are maintained in the water-to-air boundary. This configuration of the micro-spheres avoids the presence of surface adhesion forces as the micro-spheres are not in contact with the bottom of the arena. The contained liquid forms a meniscus at the center of the arena. Thus, to reduce this liquid deformation the arena size is increased and only a parcel of the arena is observed. The particles are observed by a camera with a 100 ms image period, fitted with a microscope objective.

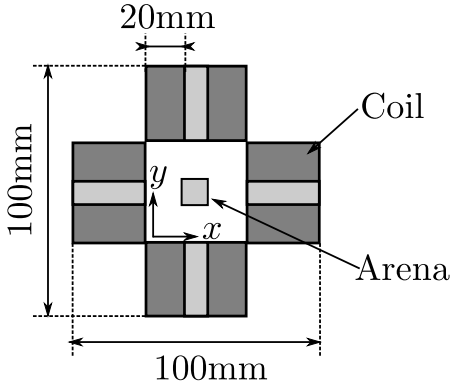

(a) Scheme of the system, four coils surrounding an arena [22].

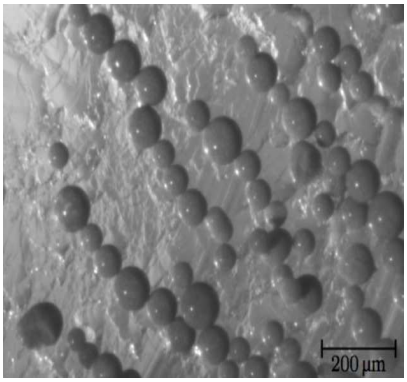

(b) Picture of the controlled paramagnetic particles [22].

Fig. 10 Design of the paramagnetic particles controlling system.

5.2 Micro-robot actuation

As the particles are made of a paramagnetic material, they exhibit a particular behavior under the influence of a magnetic field. The magnetic forces Eq. (3) on these particles depend on the gradient field squared. Besides, the micro-spheres are held in the water-to-air layer by capillary forces, hence it is assumed the only force opposing the micro-spheres' movement is the drag force induced by the liquid environment. The drag force increases with the velocity of the particle, thus the maximum speed of the particle is reached when the magnetic force equals the drag force.

5.3 Motion control

The control of paramagnetic particles relies on using a tracking algorithm to detect particle motion. To benefit from a fast detection method, the tracking algorithm uses a region of interest, the center of which is either defined by the user or assumed to be the last position of the particle. Moreover, to overcome the lighting disturbances, an adaptive thresholding is then applied on this region. Afterwards, an erosion filter is applied to reduce noise on the frame. As several micro-particles are used once in a time, the particle is assumed to be the biggest object on the frames. A size test is also applied to verify that the detected particle has an acceptable size, otherwise the particle is considered lost. In the experiment, the environment was carefully prepared to avoid any disturbances. The image processing algorithm reaches its limit when several particles are used and more than one particle is in the region of interest : the algorithm returns an inexact position, which is the average of the particle positions inside the region.

The tracking algorithm provides PI [6] controllers - one for each axis (x,y) - with the difference between the actual position and the desired position of the particle. The PI controllers have the same gains for each axis Fig. 11.

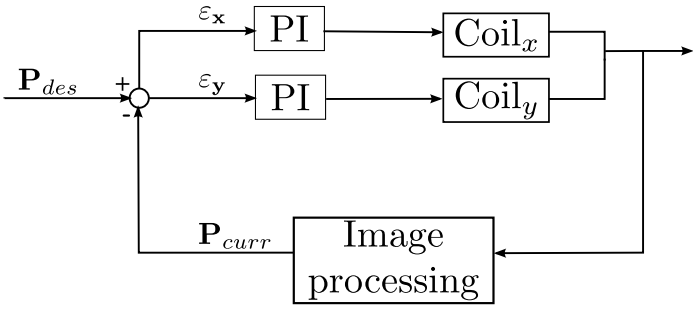

Fig. 11 Schematic diagram of the control loop. Two PI controllers are used to control the particle in both X and Y directions.

5.4 Experimental results and discussion

The experiments demonstrated in [22] show that controlling a particle towards a position takes around 15 s to reach a steady state. The current intensity applied to the coils is 0.8 A which generates a gradient field squared of 1.8 $\text{mT}^2.\text{m}^{-1}$. Under this condition, the speed of a particle of 100 μm is 235 $\mu\text{m.s}^{-1}$. Fig. 12(a) represents the positioning of a particle, the standard deviation according to x and y is about 8.4 μm. Fig. 12(b) shows movement of a particle around a path of preset points. The movement of the particle is not smooth due to significant overshoot in particle positioning. Moreover, it is assumed that the controlled particles are always held in the air-to-water boundary, avoiding buoyancy forces. Thus, the experiments need to be carefully prepared, otherwise the proposed model of the system is not valid anymore.

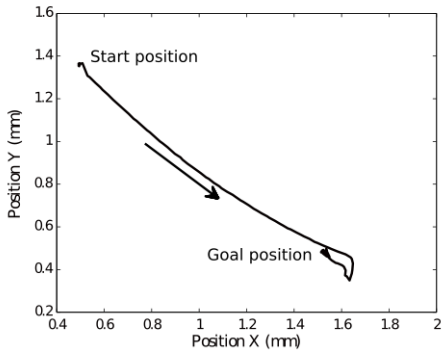

(a) Positioning of a particle according to x and y directions [22] .

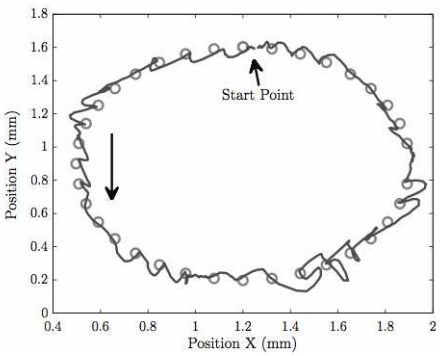

(b) The particles following a preset of points. The path is obtained from the image processing algorithm [22] .

Fig. 12 The control system performance in (a) positioning and in (b) following preset point paths.

[6] Proportional Integrator

6 MagPieR (Magnetic Piezo Robot)

6.1 Micro-robot design

The MagPieR is a micro-parallelepiped [35], composed of two heterostructure layers: a ferromagnetic material (Nickel) layer for magnetic driving on top of a bulk of PMN-PT ($Pb(Mg_{1/3}Nb_{2/3})O_3$-$PbTiO_3$: a composite of Lead-Magnesium-Niobium-Titane), a piezoelectric material used to overcome surface friction Fig. 13(a).

The MagPieR is fabricated by electrodeposition of a Ni layer on PMN-PT substrate and then by saw dicing into small rectangular samples. In the Ni layer two trenches are cut in order to align the micro-robot with the magnetic field along the trenches. The MagPieR moves inside a capacitor. The bottom electrode is the arena substrate itself,

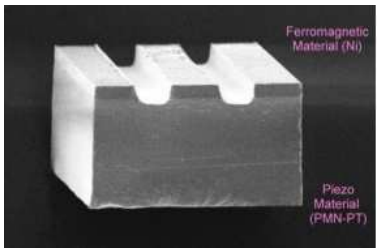

(a) Image from Scanning Electronic Microscope of MagPieR [35]

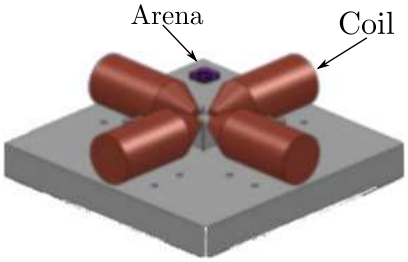

(b) Disposition of the coils surrounding the MagPieR arena [35]

Fig. 13 The MagPieR design

and the top electrode is an optically transparent conductive glass (ITO glass) allowing a visualization of the scene from above. The observation of the MagPieR is done by a top situated high speed camera (1000 frames per second). The micro-robot then moves in a dry environment. The arena is surrounded by four identical electromagnets Fig. 13(b), the coils require less than 1 A to activate the micro-robot. The coils generate a magnetic field that allows 3 DoF to the micro-robot: 2 translations in the x and y directions, and a rotation in the -x,y- plane.

6.2 Micro-robot actuation

At the micro scale, the surface adhesion force is the main factor limiting the movement of a micro-device in the air. To overcome this force the MagPier uses vertical vibration. High frequency, high voltage pulses on the bottom electrode actuate the piezoelectric effect to free the micro-robot from adhesion Fig. 14(a).

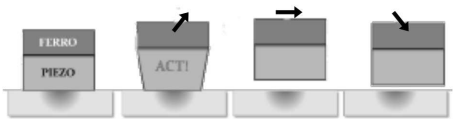

(a) Externally induced vibration actuation [35] .

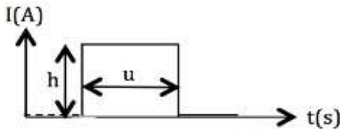

(b) Signal current sent to the coil [35] .

Fig. 14 MagPieR actuation

In-plane motion (translations and rotation) is then obtained by applying an external magnetic field generated by the coil. Only one electromagnet at a time is used to actuate the robot. The magnetic field gradient induces a magnetic force according to Eq. (1), which results in the micro-robot's translation. The magnetic field exerts a magnetic torque on the micro-robot by Eq. (2) orientating the robot in a given direction. The signal input to the coils is an impulse Fig. 14(b). The velocity of the micro-robot varies according to the amplitude h and length u of this impulse.

6.3 Motion control

The behavior of the MagPieR is identified experimentally, thus the relation between the current intensity and the displacement of the micro-robot is known. As the micro-robots operates in a dry environment, adhesion forces are predominant and influence the model of the system. In fact, the adhesion forces vary throughout the surface of the arena at this scale, hence it is difficult to simulate the micro-robot behavior with a high resolution. The controller is based on driving the micro-robot to a region the center of which is the desired position. The boundaries of this region are marked by X_{min}/X_{max} and Y_{min}/Y_{max}, which are preset values obtained by the identification of the system. In this work, the visual feedback returns an (x,y) position of the micro-robot in the workspace. The difference between the current position and the desired position is given to the PID controllers. The same PID controller is used for each coil. Moreover, every coil controls the micro-robot in one direction on a given (x-y) axis. Once the position error is given to the controller, for each axis the controller activates a coil, depending on the range of the error. Usable control laws are thus limited; simultaneous control of several coils should improve the motion of the MagPieR. Depiction Fig. 15 represents the block diagram of the controlling system.

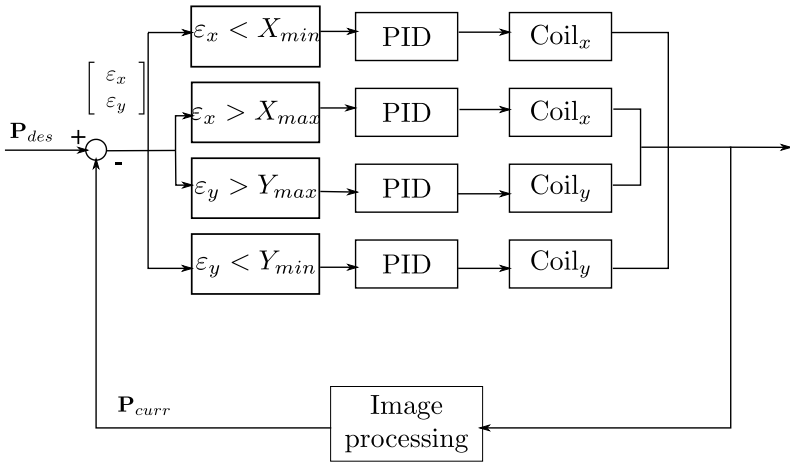

Fig. 15 Controlling scheme of the MagPieR

6.4 Experimental results and discussion

The MagPieR showed good velocity performance, indeed it won the "2mm dash" competition twice at the NIST IEEE Mobile Microrobotics Challenge, being the fastest micro-robot by performing the 2 mm race in 15 ms. Fig. 16(a)represents the resulting response of serving the MagPier to an x-y position. The figure demonstrates clearly that the x and y variables are coupled. For example, at time 100 ms, the x position has reached its desired position but the y position has not. When a signal is sent to reduce the y error, the generated magnetic force is in fact oblique and leads to an additional movement of the micro-robot in the x direction.

The second figure Fig. 16(b) shows the control of the micro-robot through an ∞-shaped trajectory. The simulated trajectory is the continuous line, and the experimental trajectory is the dotted line. The difference between the trajectories is due to the coupling of the -x,y- directions. Moreover, the control scheme is based upon reaching a region rather than a trajectory, the resulting motion is irregular and lacks precision. The use of the gradient magnetic field in a dry environment allows the micro-robot to experience high accelerations, though significant non-linearities induced by this environment limit motion accuracy. Moreover, the close arrangement of the coils leads to large field gradients, but also leads to nonlinear field distributions. Thus, accurate control of the micro-robot is hard to achieve.

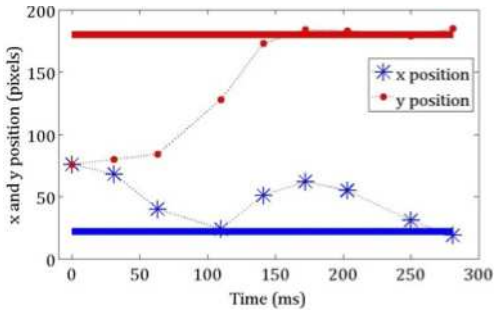

(a) Time responses to an x-y step input. The solid line is the desired position and the dashed line is the experimental result [35] .

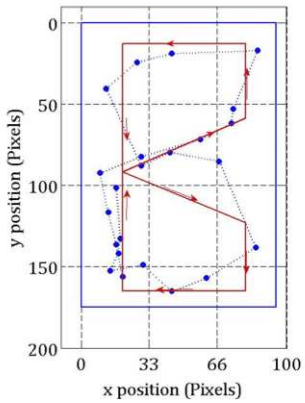

(b) An ∞-shaped controlled trajectory of the micro-robot, the solid line is the planned trajectory and the dashed one is the trajectory executed by the robot [35] .

Fig. 16 MagPieR control results. One pixel is ~ 20 μm

7 Comparison and conclusion

Characteristics of the previously presented magnetic micro-robots are summarized in Tab. 2. Magnetic actuated micro-robots are made of ferromagnetic or paramagnetic materials. The shape is designed according to the application, and the robots usually have parallelepiped, cylinder or claw geometries. The above systems' coil setups respect the same configuration : four orthogonal electromagnets are used to produce 2D in plane motion; out of planes can be added to increase the DoF of the micro-robots or to perform 2D using only the magnetic torques. Besides, the average magnetic field strength generated by the considered systems is sufficient to induce motion in the magnetic micro-robot (~10 mT). Some systems use ferromagnetic cores in their coils to increase the magnetic field strength, though the saturation of the core needs to be taken into consideration in these systems. The maximum current intensity admissible by a coil typically increases with its dimensions. However, the coils are subjected to excessive heating, and require a cooling system when a significant gradient field is needed.

The systems presented above use several types of actuation signals, such as continuous or periodic signals. Magnetic actuated micro-robots are mainly based on the gradient of the magnetic field which induces magnetic forces to translate the micro-device, the magnetic field being used to produce its orientations. However, the translation of micro-robots can also be induced by magnetic torques, which requires lower magnetic field strengths but generates limited velocities. In a dry environment, allow micro-robot experiences high accelerations, unlike in a liquid environment where the drag forces decrease the micro-robot velocity. Although, in a dry environment the adhesion forces are significant and lead to non-linearity in the system in addition to the non-linearity of the magnetic field distribution. For most of the systems, the dynamic model of the micro-robot is computed theoretically and corrected with experimental data.

Micro-robotic systems show high velocities compared to their reduced size. The controllers of the above systems perform a relatively accurate positioning, though the following of trajectories presents highly discontinuous behavior and irregularities. The control systems are, for the moment, insufficient to lead repeatable tasks at a high speed with a high reliability. The dynamics of the magnetic field and the micro-robot, established in an experimental way, do not reliably represent the micro-robot's behavior and non linearities.

The next challenges for untethered magnetic micro-robots are to benefit from 6 DoF navigation to fully explore the environment, and to be less sensitive to atmospheric variations. The coil setups can also benefit from optimized configurations in order to improve the time response in generating the magnetic field and to increase the workspace of the micro-robot. In the future, these untethered micro-robots will have a great potential for many medical, biological and industrial applications, thanks to their tiny size, wireless power and control.

Micro-robot	Mag-μBot	OctoMag	Paramagnetic Sphere	MagPieR
Micro-robot shape	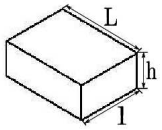	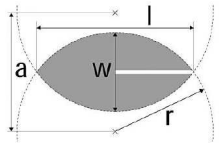	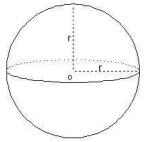	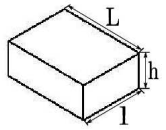
Material	NdFeB	Ni	Iron-oxide	PMN-PT + Ni
Environment	Dry/Wet	Wet	Wet	Dry
Micro-robot dimension [μm]	L=130 ± 10 h=100 ± 10 l=250 ± 10	l = 500 a= 375 w= 250	r = 60 ~ 110	L= 388 h=300 (100 of Ni) l=230
Coil number	6	8	4	4
Number of DoF	3	5	2	3
Coils position		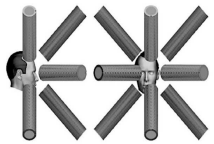	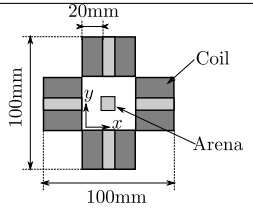	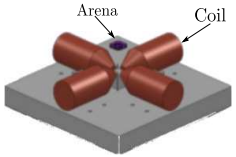
Workspace size [mm x mm]	20x20	~20x~20	10x10	20x35
Coils dimension [mm]	d_inner= – d_outer = – l = –	d_inner = 44 d_outer = 63 l = 210	d_inner = 10 d_outer = 39 l = 30	d_inner = 4 d_outer = 11 l = 17
Average magnetic field strength [mT]	15	15	6	15
Coils core	Air	VACOFLUX 50	–	Ferromagnetic
Movement equation	2	1	3	1
Current Signal	Periodic Waveform	Continuous	Continuous	square pulse
Current Intensity [A]	3	15	0.8	≤1
Velocity [mm.s^{-1}]	25	~1.9	0.235	133

Table 2 Summary of the magnetic micro-robots

References

1. Bradley J. Nelson, Ioannis K. Kaliakatsos, and Jacob J. Abbott. Microrobots for minimally invasive medicine. *Annual Review of Biomedical Engineering*, 12:55–85, June 2010.
2. Bruce R. Donald, Christopher G. Levey, Craig D. Mcgray, Igor Paprotny, and Daniela Rus. An untethered, electrostatic, globally controllable mems micro-robot. *Journal of Microelectromechanical Systems*, 2006.
3. Mohamed Kharboutly, Michaël Gauthier, and Nicolas Chaillet. Modeling the trajectory of a micro particle in a dielectrophoresis device. *IEEE International Conference on Robotics and Automation (ICRA'10)*, 2010.
4. Wuming Jing, Xi Chen, Sean Lyttle, Zhenbo Fu, Yong Shi, and David J. Cappelleri. A magnetic thin film microrobot with two operating modes. In *IEEE International Conference on Robotics and Automation (ICRA'11)*, pages 96–101, 2011.
5. Gábor Kósa, Moshe Shoham, and Menashe Zaaroor. Propulsion Method for Swimming Microrobots. *IEEE Transactions on Robotics*, 2007.
6. Li-Anne Liew, Victor M. Bright, Martin L. Dunn, John W. Daily, and Rishi. Raj. Development of SiCN ceramic thermal actuators. *IEEE International Conference on Micro Electro Mechanical Systems*, 2002.
7. David G. Cahill, Wayne K. Ford, Kenneth E. Goodson, Gerald D. Mahan, Humphrey J. Majumdar, Arunand Maris, Roberto Merlin, and Simon R. Phillpot. Nanoscale thermal transport. *Journal of Applied Physics*, 2003.
8. Yves Bellouard. *Micro-robotics: Methods and Applications*. CRC Press, 2009.
9. Sylvain Martel, Charles C. Tremblay, Serge Ngakeng, and Guillaume Langlois. Controlled manipulation and actuation of micro-objects with magnetotactic bacteria. *Applied Physics Letters*, 2006.
10. Sylvain Martel, Mahmood Mohammadi, Ouajdi Felfoul, Zhao Lu, and Pierre Pouponneau. Flagellated magnetotactic bacteria as controlled mri-trackable propulsion and steering systems for medical nanorobots operating in the human microvasculature. *The International Journal of Robotics Research*, 2009.
11. Kazuhisa Onda and Fumihito Arai. Parallel teleoperation of holographic optical tweezers using multi-touch user interface. *IEEE International Conference on Robotics and Automation (ICRA'12)*, 2012.
12. Sagar Chowdhury, Petr Svec, Wang Chenlu, Wolfgang Losert, and Satyandra K. Gupta. Gripper synthesis for indirect manipulation of cells using Holographic Optical Tweezers. *IEEE International Conference on Robotics and Automation (ICRA'12)*, 2012.
13. Jacob J. Abbott, Kathrin E. Peyer, M. C. Lagomarsino, Li Zhang, Lixin X. Dong, Ioannis K. Kaliakatsos, and Bradley J. Nelson. How Should Microrobots Swim? *International Journal of Robotics Research*, 2009.
14. Arthur W. Mahoneya, John C. Sarrazinb, Eberhard Bambergb, and Jake J. Abbottb. Velocity Control with Gravity Compensation for Magnetic Helical Microswimmers. *Advanced Robotics*, 2011.
15. Ambarish Ghosh and Peer Fischer. Controlled Propulsion of Artificial Magnetic Nanostructured Propellers. *Nano Letters*, 2009.
16. Soichiro Tottori, Li Zhang, Famin Qiu, K. Krawczyk, A. Franco-Obregón, and Bradley J. Nelson. Magnetic Helical Micromachines: Fabrication, Controlled Swimming, and Cargo Transport. *Advanced Materials*, 2012.
17. Aya Yamazaki, Masahiko Sendoh, Kazushi Ishiyama, Ken Ichi Arai, Ryutaro Kato, Masaki Nakano, and Hirotoshi Fukunaga. Wireless micro swimming machine wiht magnetic thin film. *Journal of Magnetism and Magnetic Materials*, 2004.
18. Li Zhang, Jacob J. Abbott, Lixin X. Dong, Bradley E. Kratochvil, Dominik J. Bell, and Bradley J. Nelson. Artificial Bacterial Flagella: Fabrication and Magnetic Control. *Applied Physics Letters*, 2009.
19. Masaya Hagiwara, Tomohiro Kawahara, Lin Feng, Yoko Yamanishi, and Fumihito Arai. On-chip enucleation of oocyte by magnetically driven microtools with ultrasonic vibration. *IEEE International Conference on Robotics and Automation (ICRA'11)*, 2011.
20. Chytra Pawashe, Steven Floyd, and Metin Sitti. Modeling and experimental characterization of an untethered magnetic micro-robot. *The International Journal of Robotic Research*, 28:1077–1094, August 2009.
21. Michael Kummer, Jacob J. Abbott, Bradley E. Kratochvil, Ruedi Borer, Ali Sengul, and Bradley J. Nelson. Octomag: An electromagnetic system for 5-dof wireless micromanipulation. *IEEE Transactions on Robotics*, 26(6):pp. 1006–1017, September 2010.
22. Jasper D. Keuning, Jeroen de Vries, Leon Abelmann, and Sarthak Misra. Image-based magnetic control of paramagnetic microparticles in water. In *IEEE International Conference on Intelligent Robots and Systems (IROS'11)*, pages 421–426, 2011.
23. David Folio, Christian Dahmen, Tim Wortmann, M. Arif Zeeshan, Kaiyu Shou, Salvador Pane, Bradley J. Nelson, Antoine Ferreira, and Sergej Fatikow. MRI magnetic signature imaging, tracking and navigation for targeted micro/nano-capsule therapeutics. *IEEE International Conference on Intelligent Robots and Systems (IROS'11)*, 2011.
24. Karim Belharet, David Folio, and Antoine Ferreira. Three-Dimensional Controlled Motion of a Microrobot using Magnetic Gradients. *Advanced Robotics*, 2011.
25. Sylvain Martel, Ouajdi Felfoul, Jean-Baptiste Mathieu, Arnaud Chanu, Samer Tamaz, Mahmood Mohammadi, Martin Mankiewicz, and Nasr Tabatabaei. MRI-based Medical Nanorobotic Platform for the Control of Magnetic Nanoparticles and Flagellated Bacteria for Target Interventions in Human Capillaries. *The International Journal of Robotic Research*, 2009.
26. Zoltan Nagy, Olgac Ergeneman, Jacob J. Abbott, M. Hutter, A. M. Hirt, and Bradley J. Nelson. Modeling Assembled-MEMS Microrobots for Wireless Magnetic Control. *IEEE International Conference on Robotics and Automation (ICRA'08)*, 2008.
27. Stefano Palagi, Virginia Pensabene, Lucia Beccai, Barbara Mazzolai, Arianna Menciassi, and Paolo Dario. Design and development of a soft magnetically-propelled swimming microrobot. *IEEE International Conference on Robotics and Automation (ICRA'11)*, 2011.
28. Steven Floyd, Chytra Pawashe, and Metin Sitti. Dynamic modeling of stick slip motion in an untethered magnetic micro-robot. In *Robotics: Science and Systems*. The MIT Press, 2009.
29. Guan-Lin Jiang, Yunn-Horng Guu, Chiang-Ni Lu, Pei-Kao Li, Hui-Mei Shen, Lung-Sheng Lee, Jerliang Andrew Yeh, and Max Ti-Kuang Hou. Development of rolling magnetic microrobots. *Journal of Micromechanics and Microengineering*, 2010.
30. Karl Vollmers, Dominic R. Frutiger, Bradley E. Kratochvil, and Bradley J. Nelson. Wireless resonant magnetic microactuator for untethered mobile microrobots. *Applied Physics Letters*, 2008.
31. Dominic R. Frutiger, Karl Vollmers, Bradley Kratochvil, and Bradley J. Nelson. Small, Fast, and Under Control: Wireless Resonant Magnetic Micro-agents. *International Journal of Robotics Research*, 2010.
32. Hsi-Wen Tung, Dominic R. Frutiger, Salvador Pane, and Bradley J. Nelson. Polymer-based Wireless Resonant Magnetic microrobots. *IEEE International Conference on Robotics and Automation (ICRA'12)*, 2012.
33. Raju V. Ramanujan and Y. Y. Yeow. Synthesis and characterisation of polymer-coated metallic magnetic materials. *Materials Science and Engineering*, 2005.
34. Pierre Pouponneau, L'Hocine Yahia, Yahye Merhi, Laura Mery Epure, and Sylvain Martel. Biocompatibility of candidate materials for the realization of medical microdevices. *IEEE International Conference of the Engineering in Medicine and Biology Society*, 2006.

35. Alexander I. Ivan, Gilgueng Hwang, Joël Agnus, Micky Rakotondrabe, Nicolas Chaillet, and Stéphane Régnier. First experiment on magpier : a planar wireless magnetic and piezoelectric microrobot. In *IEEE International Conference on Robotics and Automation (ICRA'11)*, pages 102 – 108, 2011.
36. Semi Jeong, Hyunchul Choi, Seong Young Ko, Jong-oh Park, and Sukho Park. Remote Controlled Micro-Robots Using Electromagnetic Actuation (EMA) Systems. *IEEE International Conference on Biomedical Robotics and Biomechatronics*, 2012.
37. Masaya Hagiwara, Tomohiro Kawahara, Toru Iijima, Yoko Yamanishi, and Fumihito Arai. High speed microrobot actuation in a microfluidic chip by levitated structure with riblet surface. *IEEE International Conference on Robotics and Automation (ICRA'12)*, 2012.
38. Jacob J. Abbott, Zoltan Nagy, Felix Beyeler, and Bradley J. Nelson. Robotics in the Small, Part I: Microrobotics. *IEEE Robotics and Automation Magazine*, 2007.
39. Gustavo Calderon, Jean-Philippe Draye, Davor Pavisic, Roberto Teran, and Gaetan Libert. Nonlinear Dynamic System Identification with Dynamic Recurrent Neural Networks. *International Workshop on Neural Networks for Identification, Control, Robotics, and Signal/Image Processing (NICROSP '96)*, 1996.
40. Ming-Bin Li and Meng Joo Er. Nonlinear System Identification Using Extreme Learning Machine. *International Conference on Control, Automation, Robotics and Vision (ICARCV'06)*, 2006.
41. Patrick Lichtsteiner, Christoph Posch, and Tobi Delbruck. A 128*128 120 dB 15 s Latency Asynchronous Temporal Contrast Vision Sensor. *IEEE Journal of Solid-State Circuits*, 2008.
42. Eric D. Diller, Steven Floyd, Chytra Pawashe, and Metin Sitti. Control of multiple heterogeneous magnetic microrobots in two dimensions on nonspecialized surfaces. *IEEE Transactions on Robotics*, 28(1):172–182, 2012.
43. Steven Floyd, Chytra Pawashe, and Metin Sitti. An untethered magnetically actuated micro-robot capable of motion on arbitrary surfaces. *IEEE International Conference on Robotics and Automation (ICRA'08)*, 2008.
44. http://www.nist.gov/el/isd/robotals.cfm.
45. Michael Isard and Andrew Blake. Condensation - conditional density propagation for visual tracking. *International Journal of Computer Vision*, 29(1):5–28, 1998.
46. Steven M. LaValle. *Planning Algorithms*. Cambridge University Press, Cambridge, U.K., 2006. Available at http://planning.cs.uiuc.edu/.
47. Chytra Pawashe, Steven Floyd, Eric D. Diller, and Metin Sitti. Two-Dimensional Autonomous Microparticle Manipulation Strategies for Magnetic Microrobots in Fluidic Environments. *IEEE Transactions on Robotics*, 2012.
48. Steven Floyd, Chytra Pawashe, and Metin Sitti. Microparticle manipulation using multiple untethered magnetic micro-robots on an electrostatic surface. In *IEEE International Conference Intelligent Robots and Systems (IROS'09)*, pages 528–533, 2009.
49. Eric D. Diller, Chytra Pawashe, Steven Floyd, and Metin Sitti. Assembly and disassembly of magnetic mobile micro-robots towards deterministic 2-D reconfigurable micro-systems. *International Journal of Robotics Research*, 2011.
50. Kemal Berk Yeşin, Karl Vollmers, and Bradley J. Nelson. Modeling and control of Untethered Biomicrorobots in a Fluidic environment using Electromagnetic Fields. *International Journal of Robotics Research*, 2006.
51. Islam S. M. Khalil, Jasper D. Keuning, Leon Abelmann, and Sarthak Misra. Wireless magnetic-based control of paramagnetic microparticles. *IEEE International Conference on Biomedical Robotics and Biomechatronics*, 2012.